quency and ω_{ep} is the electronic plasma frequency. When the wires do not maintain electrical continuity, as in these experiments, $\omega_{eo} > 0$.

In particular, over the band of frequencies that have been previously identified as the left-handed propagation region (ε and μ both negative, about 10.2 to 10.8 GHz), the index is expected to take very negative values on the low-frequency side of the left-handed band, passing through a value of zero on the high-frequency side. The measured index as a function of frequency for the LHM sample is presented (Fig. 4) and compared with theoretical predictions and similar data taken on the Teflon sample. Although the measured index for Teflon is basically flat across the X-band frequency range, the index of refraction for the LHM is negative over the left-handed frequency band and is highly dispersive, in a manner consistent with theoretical predictions (*7*). We used Eqs. 1 and 2 to calculate the theoretical curves using the following parameters: $f_{mp} = 10.95$ GHz, $f_{mo} = 10.05$ GHz, $f_{ep} = 12.8$ GHz, $f_{eo} = 10.3$ GHz, and $\gamma = 10$ MHz ($f = \omega/2\pi$).

We note two limitations on our experimental technique that prevent us from probing the effective index corresponding to the extremes of the left-handed frequency band. When the effective index approaches zero, the wavelength in the LHM becomes very large, presumably larger than the dimensions of the sample. Under these conditions, the sample is best characterized by a scattering cross section rather than interpreted with geometrical ray concepts. Thus, we are unable to unambiguously determine the index in the frequency region from about 10.8 to 12 GHz, which would correspond to an imaginary index rather than positive as measured. This limitation might be eased by the use of thicker and wider samples. Also, because we cut our refraction interface to be roughly 18.4° from normal incidence, when $|n| \gtrsim 3$, we expect the incident beam to undergo total internal reflection rather than refraction, possibly explaining the lack of observed index values below -3 and above $+3$.

An immediate question is whether the negative index-of-refraction property can be implemented at optical frequencies. It is unlikely that the inherent material properties of conductors will scale much past the infrared, rendering left-handed materials, such as those used here, ineffective. The phenomenon of negative refraction has recently been predicted by numerical simulations on dielectric, photonic crystals, at certain frequencies near negative group-velocity bands (*10*, *11*). Although the refracted beam may bend toward a negative angle in these systems, it is difficult to define an equivalent index of refraction with the same generality as we find in metamaterials, because these effects occur above the Bragg reflection frequency. Furthermore, surface waves at the interface between photonic crystals and other uniform media complicate the surface matching problem, making design considerations more difficult. Nevertheless, the use of photonic crystals as negative refractive materials is intriguing and may offer the means of extending the phenomenon we report here to optical wavelengths. Any material that exhibits the property of negative refractive index, a property not observed in naturally occurring materials, will have a variety of practical applications, such as beam steerers, modulators, band-pass filters, and lenses permitting subwavelength point source focusing.

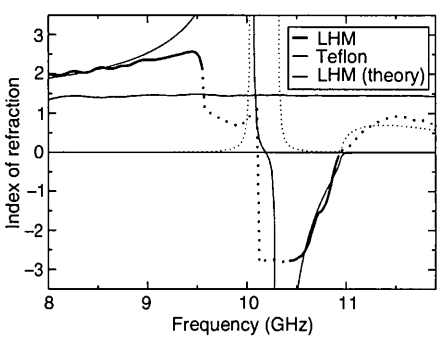

Fig. 4. Index of refraction versus frequency. The blue curve corresponds to data from the Teflon sample, and the black curve is for the LHM data. The dotted portions of the LHM curve indicate regions where the index is expected to be either outside our limit of detection ($|n| > 3$) or dominated by the imaginary component and therefore could not be reliably determined experimentally. The solid red curve is the real component, and the dotted red curve is the imaginary component of the theoretical expression for the refractive index as fit to the square root of the product of Eqs. 1 and 2 as described in the text.

References and Notes

1. V. G. Veselago, *Sov. Phys. Usp.* **10**, 509 (1968).
2. J. B. Pendry, *Phys. Rev. Lett.* **85**, 3966 (2000).
3. D. R. Smith, W. J. Padilla, D. C. Vier, S. C. Nemat-Nasser, S. Schultz, *Phys. Rev. Lett.* **84**, 4184 (2000).
4. R. A. Shelby, D. R. Smith, S. C. Nemat-Nasser, S. Schultz, *Appl. Phys. Lett.* **78**, 489 (2001).
5. J. B. Pendry, A. J. Holden, D. J. Robbins, W. J. Stewart, *IEEE Trans. Microwave Theory Tech.* **47**, 2075 (1999).
6. J. B. Pendry, A. J. Holden, W. J. Stewart, I. Youngs, *Phys. Rev. Lett.* **76**, 4773 (1996).
7. D. R. Smith, N. Kroll, *Phys. Rev. Lett.* **85**, 2933 (2000).
8. R. A. Shelby, D. R. Smith, S. Schultz, data not shown.
9. L. D. Landau, E. M. Lifshitz, L. P. Pitaevskii, *Electrodynamics of Continuous Media* (Butterworth-Heinenann, Oxford, UK, ed. 2, 1984), p. 287.
10. M. Notomi, *Phys. Rev. B* **62**, 10696 (2000).
11. B. Gralak, S. Enoch, G. Tayeb, *J. Opt. Soc. Am. A* **17**, 1012 (2000).
12. We thank R. Greegor and C. Parazzoli from Boeing for helpful discussions. This research was supported by the Defense Advanced Research Projects Agency (DARPA) (contract DAAD19-00-1-0525), by DARPA through a grant from the Office of Naval Research (contract N00014-00-1-0632), and by the Air Force Office of Science Research (grant F49620-00-1-0380).

8 January 2001; accepted 22 February 2001

Three-Dimensionally Ordered Array of Air Bubbles in a Polymer Film

Mohan Srinivasarao,[1]* David Collings,[2] Alan Philips,[3]† Sanjay Patel[4]

We report the formation of a three-dimensionally ordered array of air bubbles of monodisperse pore size in a polymer film through a templating mechanism based on thermocapillary convection. Dilute solutions of a simple, coil-like polymer in a volatile solvent are cast on a glass slide in the presence of moist air flowing across the surface. Evaporative cooling and the generation of an ordered array of breath figures leads to the formation of multilayers of hexagonally packed water droplets that are preserved in the final, solid polymer film as spherical air bubbles. The dimensions of these bubbles can be controlled simply by changing the velocity of the airflow across the surface. When these three-dimensionally ordered macroporous materials have pore dimensions comparable to the wavelength of visible light, they are of interest as photonic band gaps and optical stop-bands.

A variety of templating methods that use self-assembly can create structures with submicrometer dimensions. These methods include templating using ordered arrays of colloidal particles (*1*–*5*), templating using an emulsion (*6*), honeycomb structures formed by polymers with rod-coil architecture (*7*–*10*), self-organized surfactants such as mesoporous silica (*11*–*13*), microphase-separated block copolymers (*14*–*16*), and even bacteria (*17*). Recent developments using colloidal crystal templating allow the preparation of ordered macroporous materials that have three-dimensional (3D) ordering of pores

with dimensions of tens to thousands of nanometers (*1–5*).

With macroporous materials formed by colloidal crystal templating (*1–5*), colloidal crystals of polystyrene or silica spheres are infiltrated with a fluid that fills and solidifies in the vacant space between the spheres. In a subsequent step, the templating spheres are removed by either thermal decomposition or solvent extraction, thus creating a solid skeleton that contains a 3D array of pores whose dimensions match those of the templating spheres. It is obvious that the dominant length scale of the porous solid formed by such methods is "built in" by the template used, thus making dynamic control of the length scale virtually impossible.

Here, we report a simple and robust method that uses evaporative cooling to form ordered structures with dimensions that can be controlled from about 0.20 to 20 μm. The ordered structures are formed by evaporating solutions of a simple coil-like polymer in a volatile solvent, in the presence of moisture with forced airflow across the solution surface. A hexagonally packed array of holes then forms on the surface of the polymer. When a solvent less dense than water is used, such as benzene or toluene, the hexagonal array propagates through the film. In contrast, in samples generated from a solvent more dense than water, such as carbon disulfide (CS_2), only a single layer of pores is formed and a 3D array is not produced, contrary to previous reports (*7, 8, 18*). Our results show that water may play a key role in the templating system reported here, as well as in other templating systems (*7, 8*). The polymer we used is polystyrene (atactic with weight-average molecular weight of 50,000; Scientific Polymer Products, New York) with one end terminated by a carboxylic acid group [referred to as a monochelic polymer (*19*)], with a typical concentration in solution ranging from 0.1 to 5% by weight.

These ordered structures are readily formed upon placing a drop of polystyrene solution on a microscope slide in a moist atmosphere with airflow across the surface. Within several seconds, the solvent evaporates and leaves behind an ordered array of holes on the solid polymer surface (Fig. 1). We examined these structures by conventional transmitted light and laser scanning confocal microscopy as well as scanning electron microscopy. Such films display bright iridescent colors when viewed with reflected light (Fig. 1A), indicative of a periodic refractive index variation through the thickness of the film. At high magnification, highly ordered structures with hexagonal packing are evident on the surface of the film (Fig. 1B), with slight imperfections sometimes apparent (Fig. 1C). The diffraction pattern obtained from the film also shows the expected hexagonal symmetry (Fig. 1D).

We used conventional light microscopy to optically section the film shown in Fig. 1. The film exhibits ordered structure throughout its thickness (Fig. 2). Optical sections at 2.55-μm intervals in the *z* direction (the direction normal to the film's surface) show hexagonal packing of spheres around the defect in several layers, but beyond 10 μm into the film, the defect disappears. This demonstrates 3D order where each layer of the ordered structure is distinct from the subsequent layer.

The 3D nature of these films is also evident in reflected light confocal microscopy (Fig. 3). The left side of Fig. 3 shows selected optical sections taken in the *xy* plane at varying depths into a film. Although sphere size is about 2 μm, ordered arrays of spheres are present at depths greater than 10 μm from the film's surface (Fig. 3C), including a packing discontinuity at around 5 μm (Fig. 3B). When the same location is subjected to optical sectioning in the *xz* plane, multiple reflective layers are also clearly present at intervals of around 2 μm, consistent with the observed hole size (Fig. 3, A′ to C′). Image analysis software allowed the confocal data set of the *xz* optical sections to be rotated through 90°. This transformation generated all aspects of

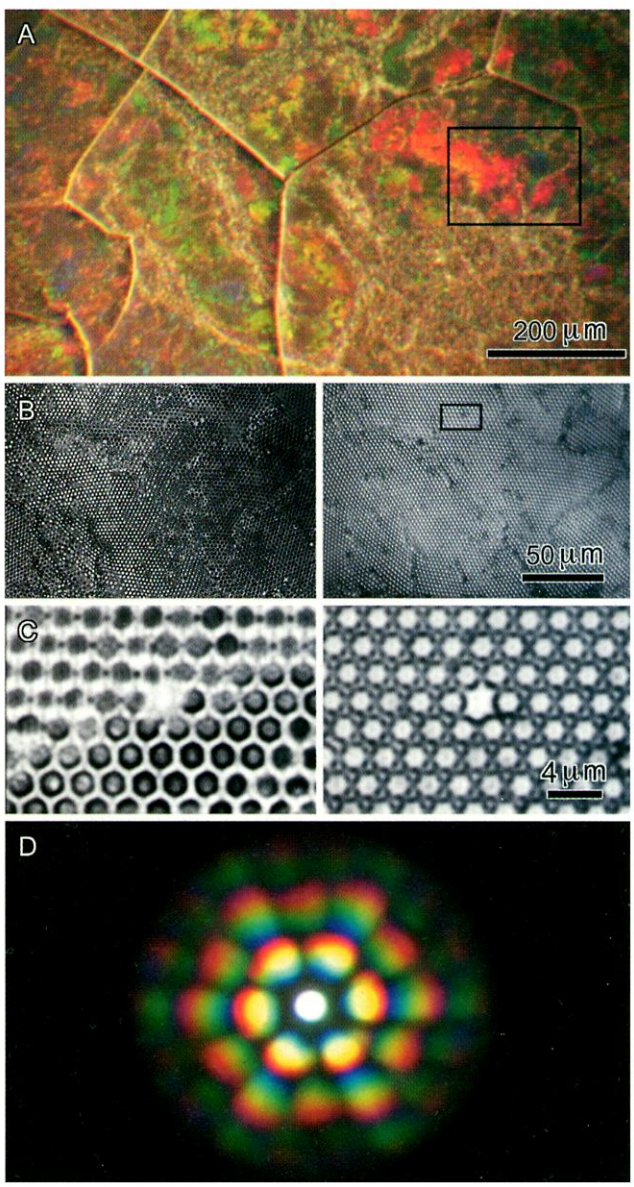

Fig. 1. Polystyrene films with hexagonally ordered arrays of air holes. (**A**) Reflected white light from a polystyrene film shows interference colors in patches across the film, along with occasional cracks in the film surface [imaged with a Leica DM12 dissecting microscope (1.6× lens) and a Hamamatsu color charge-coupled device (CCD) camera]. (**B** and **C**) Medium (B) and high magnification (C) images of areas boxed in (A) and (B), respectively, obtained with a Leica DMIRB inverted microscope (20× dry and 100× oil immersion lenses, respectively). A krypton laser (568 nm) was used as a light source for concurrent confocal reflectance (left) and transmitted bright-field imaging (condenser stopped down) (right). The film contains an ordered array of holes with diameters of about 2 μm. Occasional irregularities in packing can be seen at high magnification. (**D**) The diffraction pattern from the film in the region shown around the discontinuity shows the expected hexagonal symmetry (imaged with 100× NA 1.4 oil immersion lens; Bertrand lens, color CCD camera). Images in this and other figures were processed through Adobe Photoshop.

[1]School of Textile and Fiber Engineering and School of Chemistry and Biochemistry, Georgia Institute of Technology, Atlanta, GA 30332, USA. [2]Department of Botany, North Carolina State University, Raleigh, NC 27695, USA. [3]Department of Textile Engineering, Chemistry and Science, North Carolina State University, Raleigh, NC 27695, USA. [4]Bell Laboratories, Lucent Technologies, Murray Hill, NJ 07974, USA.

*To whom correspondence should be addressed. E-mail: mohan@tfe.gatech.edu

†Present address: Department of Polymer Science, University of Southern Mississippi, Hattiesburg, MS 39406, USA.

the original *xy* optical stack shown in Fig. 3, A to C, including the inhomogeneity in Fig. 3B. Similarly, data from the optical series of *xy* planes could be transformed into the vertical data of the *xz* planes, and this transformation showed the 2-μm periodicity of reflective planes (*20*).

Having shown that the structure of the polymer film consists of ordered 3D arrays of holes or air pockets, we now address several consequent questions: Do these structures form in the absence of moisture? Why are the holes or air pockets uniform in size, and why are they so ordered? What is the mechanism of structure formation? And more important, can the length scale of the structure be controlled with ease?

When we repeated the experiment in the absence of moisture in the atmosphere, a solid polymer film formed, devoid of the ordered structures. Because the formation of 3D ordered arrays is critically dependent on the presence of atmospheric moisture, we would argue that the structure observed is a result of the formation and subsequent crystallization of "breath figures" (*21–28*). Breath figures form when a cold solid or a liquid surface is brought in contact with moist air. Moisture then condenses on the cold surface to form water droplets that grow with time, giving rise to distinct patterns on the surface. Breath figures have been studied in detail by Rayleigh (*21, 22*), Baker (*23*), Aitken (*24*), and more recently by Beysens, Knobler, and co-workers (*25–28*). In the initial stages of the growth process of breath figures, the droplets grow as isolated objects with no interaction between droplets, and in the late stages growth occurs by coalescence, leading to polydispersity in their size. Beysens, Knobler, and co-workers (*25, 27*) showed that it was possible to form an ordered array of water droplets on a liquid surface during the initial stages of the condensation process; the droplets do not coalesce, and hence the size of the droplets is more uniform. Limaye *et al.* (*29*) later demonstrated that when the liquid surface consists of a volatile fluid, the dynamics of the breath figures are considerably altered. Our results strongly suggest that breath figures and their crystallization are responsible for the formation of the 3D ordered macroporous array of holes on the polymer films.

Our model for the formation of ordered macroporous structures in polystyrene films is illustrated in Fig. 4. The high vapor pressure of the solvent and the velocity of air across the surface drive solvent evaporation, rapidly cooling the surface. We have measured this cooling to be as much as 25°C below room temperature, resulting in an evaporating polymer surface of near 0°C (*20*). This cooling leads to the nucleation and growth of water droplets that grow as a function of time (*25–27*). Airflow across the sur-

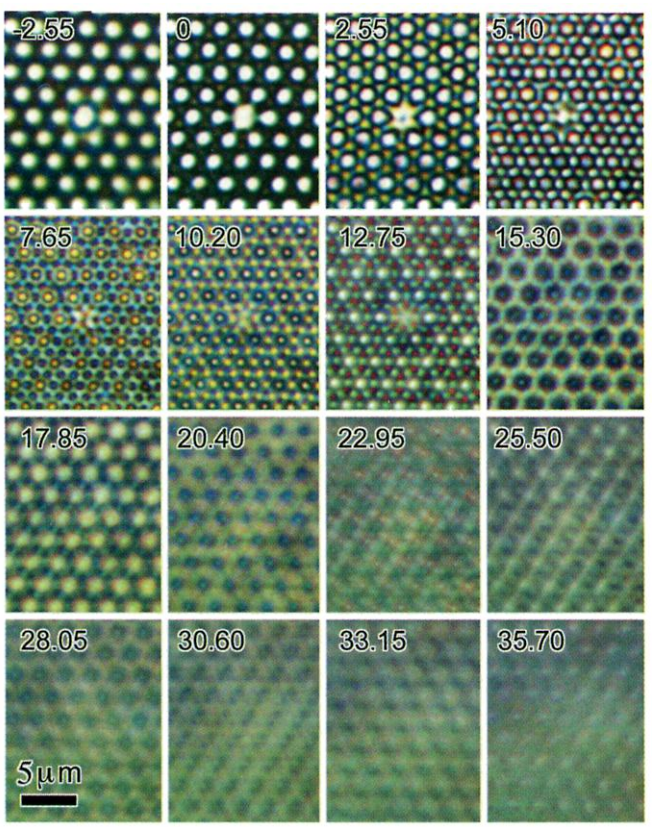

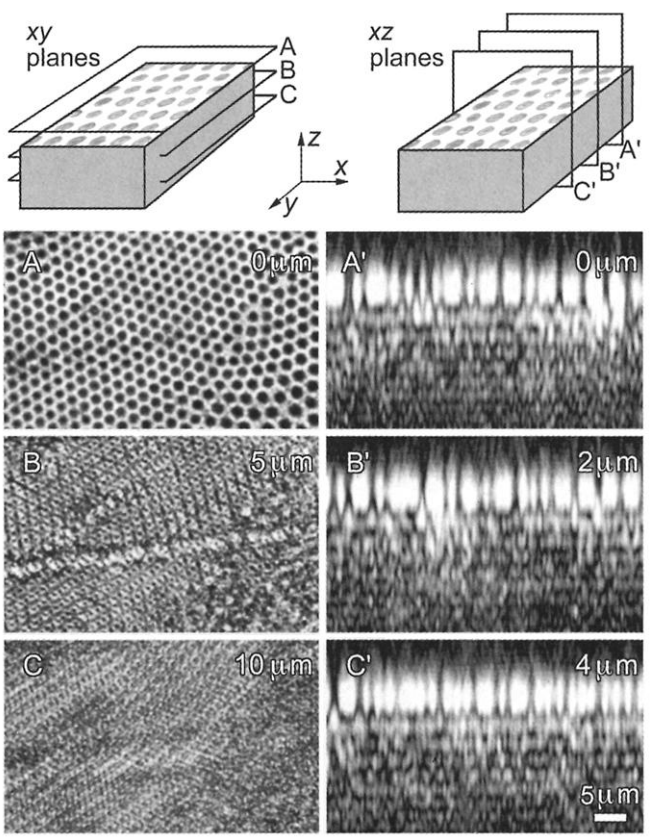

Fig. 2 (left). Polystyrene films containing multiple layers of holes. Optical sectioning (shown with depths marked relative to the film's approximate surface) of the discontinuity shown in Fig. 1C using transmitted white light. Even at 15.30 μm from the surface, 2-μm holes are still visible but the discontinuity is no longer present. **Fig. 3 (right).** Confocal optical sectioning (reflected 568-nm light, 100× NA 1.4 lens) confirms that polystyrene films contain multiple layers. Sectioning of the same region of a film with holes 2 μm in diameter was conducted in two different modes, with the image planes oriented in different directions as indicated at the top. Using the more common approach to optical sectioning (left), reflected light sections were collected from *xy* planes, with a piezoelectrode stepper motor attached to the microscope stage allowing further planes to be collected at 0.5-μm intervals in the *z* direction into the film. Three planes, whose locations are denoted by A, B, and C in the schematic, are shown in (**A**), (**B**), and (**C**) at depths of 0, 5, and 10 μm from the film's surface. Although the overall pattern of holes remains constant through the different sections, a discontinuity exists about 5 μm down into the film. In the second optical sectioning method (right), reflections were recorded in the *xz* or vertical plane by taking line scans at varying depths. Multiple optical sections were generated by moving the position of the line scan at 0.25-μm intervals along the *y* dimension. Three slices separated by 2 μm, denoted by A′, B′, and C′ in the schematic, are shown in (**A′**), (**B′**), and (**C′**). These vertical sections show multiple reflective layers in the film at 2-μm intervals, consistent with the diameter of the holes.

face, coupled with convection currents on the solution surface due to evaporation, drive the ordering or packing of the water droplets into hexagonally packed arrays. Further, these structures are analogous to the "bubble rafts" that Bragg and Nye (*30*) created using surfactant bubbles to model the motion of defects or dislocations in a crystal. A closer look at Fig. 1B reveals grain boundaries on the surface of films, similar to the bubble rafts and the packing of colloidal particles (*31*). When the surface is completely covered by water droplets, the temperature difference between the surface and the droplets eventually dissipates, and the droplets, being denser than the solvent, sink into the solution (Fig. 4). Once the solution surface is free, the whole process of evaporative cooling, water droplet condensation, and subsequent ordering repeats itself. Furthermore, the first layer of droplets can act as a template for successive layers, leading to the 3D architecture observed upon complete evaporation of the solvent. Once the film returns to ambient temperature, the condensed water and residual solvent evaporate, leaving behind the 3D polymer scaffold.

Our model has several implications for the structure of 3D ordered arrays. First, it requires that the cells be open, which we have confirmed by successfully backfilling the structures with a liquid as well as by scanning electron microscopy (*20*). The cells need to be open because the condensed water droplets need to evaporate to leave behind a hole in the solid polymer film. Second, our model depends on the solvent being less dense than water, which agrees with our observations that a 3D network forms when benzene or toluene are the solvents, whereas only 2D porous films are obtained when CS_2 is the solvent. Third, our model would suggest that the pore size should depend on the air velocity across the polymer surface, as we have observed. When the velocity increased from 30 m/min to 300 m/min, the size of the air bubbles decreased from 6 μm to 0.5 μm.

This process of forming ordered macroporous materials should be possible for many polymeric systems that are dissolved in a volatile solvent and exposed to an atmosphere containing moisture. We have been able to form such ordered structures using cellulose acetate and polymethylmethacrylate. Unlike prior studies (*7–10*), a special, complex architecture of the polymer is not necessary.

Several questions remain concerning the model shown in Fig. 4: Why do the bubbles of condensed water that eventually become the holes in the polystyrene film not coalesce during the formation of hexagonal packing, and why are the holes of similar size throughout the film? When the structure formation process is viewed through a microscope, it is remarkable to find water droplets elastically bouncing against each other without any coalescence, thus behaving as hard spheres on a surface. We believe this observation of elastic interaction provides the solution to the problem of lack of coalescence (see below), thus giving rise to the uniform size observed.

The phenomenon of liquid drops that fail to recognize and coalesce with bodies of the same liquid has long intrigued scientists, and was studied by Rayleigh as early as 1879 (*32–37*). It is now recognized that such behavior is driven by a thermocapillary convection (*38, 39*), which causes convective motion in and between the two bodies of fluid. This motion, coupled with the presence of a lubricating film of air between the drops, suppresses coalescence of the two drops as long as there is a finite temperature gradient. In the experiments described here, the solution surface is colder because of evaporative cooling, whereas the water droplets are hotter because of the latent heat of condensation. This large temperature difference will lead to a thermocapillary convection and stabilize the condensing water droplets on or at the polymer solution surface. The stability and the lack of coalescence between water droplets can also be brought about by a similar temperature gradient between the drops.

Another hypothesis that does not involve thermocapillarity can also be advanced. In this scenario, the condensing water droplets are kept apart and made to interact elastically by the vapor of the evaporating solvent as it escapes from the surface, thus providing a separating layer between the two droplets. As long as the time of interaction between the droplets is less than the time required for the vapor to escape the interstices, the two droplets will interact elastically where the vapor between the droplets supports the noncoalescence (*40*).

One important advantage of our method is the ease with which such ordered macroporous assemblies that are 3D in nature can be created using rather simple polymers. Unlike other templated self-assemblies, the size of these structures can be easily tailored and dynamically controlled within the range 0.2 to 20 μm simply by changing the velocity of airflow across the surface. The material can be used in applications such as beam steering devices, microlens arrays, or the fabrication of picoliter beakers used for the analysis of small quantities of analytes (*41–43*). Such macroporous templates can be used to form porous metals simply by chemically reducing metals onto the scaffolding that is left behind. One can condense vapors other than moisture with the aim of making ordered spherical particles. It is also possible to tune the refractive index of the scaffolding material so as to make the films suitable for photonic band gap applications (*44–47*).

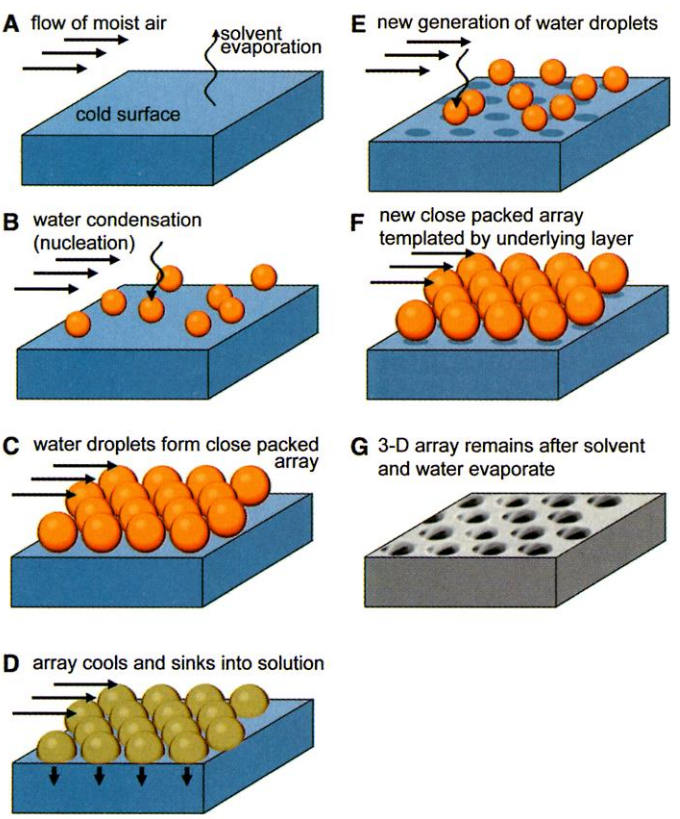

Fig. 4. A model for the formation of the structure in polymer films. The images are color-coded, with blue and orange denoting low and high temperatures, respectively, relative to room temperature. (**A**) The conditions under which the experiment is performed. (**B**) Evaporation of the solvent cools the solution surface, thus initiating the nucleation and growth of moisture. (**C**) Because of the convective currents arising from the evaporation as well as from the airflow across the surface, the water droplets pack into a hexagonal array. (**D** to **F**) We hypothesize that the ordered array sinks into the solution, thus leaving the surface of the solution free for the nucleation and growth of moisture to form another ordered array of water droplets. (**G**) When all of the solvent has evaporated, the film must return to room temperature, thus allowing the water droplets to evaporate as well while leaving behind the scaffold.

References and Notes

1. B. T. Holland, C. F. Blanford, A. Stein, *Science* **281**, 538 (1998).
2. H. Yan *et al.*, *Adv. Mater.* **11**, 1003 (1999).
3. K. M. Kulinowski, P. Jiang, H. Vaswani, V. L. Colvin, *Adv. Mater.* **12**, 833 (2000).
4. O. D. Velev, T. A. Jede, R. F. Lobo, A. M. Lenhoff, *Nature* **389**, 447 (1997).
5. A. Blanco *et al.*, *Nature* **405**, 437 (2000).
6. A. Imhof, D. J. Pine, *Nature* **389**, 948 (1997).
7. G. Widawski, B. Rawiso, B. Francois, *Nature* **369**, 387 (1994).
8. S. A. Jenekhe, X. L. Chen, *Science* **283**, 372 (1999).
9. O. Pitois, B. Francois, *Colloid. Polym. Sci.* **277**, 574 (1999).
10. ———, *Eur. Phys. J.* **B8**, 225 (1999).
11. A. Monnier *et al.*, *Science* **261**, 1299 (1993).
12. J. S. Beck *et al.*, *J. Am. Chem. Soc.* **114**, 10834 (1992).
13. C. T. Kresge, M. E. Leonowicz, W. J. Roth, J. C. Vartuli, J. S. Beck, *Nature* **359**, 710 (1992).
14. M. Park, C. Harrison, P. M. Chaikin, R. A. Register, D. H. Adamson, *Science* **276**, 1401 (1997).
15. T. L. Morkved, P. Wiltzius, H. M. Jaeger, D. G. Grier, T. A. Witten, *Appl. Phys. Lett.* **64**, 422 (1994).
16. Z. Li *et al.*, *J. Am. Chem. Soc.* **118**, 10892 (1996).
17. S. A. Davis, S. L. Burkett, N. H. Mendelson, S. Mann, *Nature* **385**, 420 (1997).
18. O. Karthaus *et al.*, *Langmuir* **16**, 6071 (2000).
19. X. F. Zhong, A. Eisenberg, *Macromolecules* **27**, 1751 (1994).
20. M. Srinivasarao, D. Collings, A. Philips, S. Patel, data not shown.
21. Lord Rayleigh, *Nature* **86**, 416 (1911).
22. ———, *Nature* **90**, 436 (1912).
23. J. T. Baker, *Philos. Mag.* **56**, 752 (1922).
24. J. Aitken, *Nature* **86**, 516 (1911).
25. D. Beysens, A. Steyer, P. Guenoun, D. Fritter, C. M. Knobler, *Phase Transitions* **31**, 219 (1991).
26. B. J. Briscoe, K. P. Galvin, *J. Phys. D* **23**, 422 (1990).
27. D. Beysens, C. M. Knobler, *Phys. Rev. Lett.* **57**, 1433 (1986).
28. F. Family, P. Meakin, *Phys. Rev. Lett.* **61**, 428 (1988).
29. A. V. Limaye, R. D. Narhe, A. M. Dhote, S. B. Ogale, *Phys. Rev. Lett.* **76**, 3762 (1996).
30. W. L. Bragg, J. F. Nye, *Proc. R. Soc. London Ser. A* **120**, 474 (1947).
31. C. D. Dushkin, K. Nagayama, T. Miwa, P. A. Kralchevsky, *Langmuir* **9**, 3695 (1993).
32. Lord Rayleigh, *Philos. Mag.* **36**, 321 (1899).
33. ———, *Proc. R. Soc. London* **28**, 406 (1879).
34. ———, *Proc. R. Soc. London* **34**, 130 (1882).
35. O. Reynolds, *Chem. News* **44**, 211 (1881).
36. J. Walker, *Sci. Am.* **238**, 123 (June 1978).
37. P. Dell' Aversana, G. P. Neitzel, *Phys. Today* **51**, 38 (1998).
38. P. Dell' Aversana, J. R. Banavar, J. Koplik, *Phys. Fluids* **8**, 15 (1996).
39. P. Dell' Aversana, V. Tontodonato, L. Carotenuto, *Phys. Fluids* **9**, 2475 (1997).
40. Although the discussion in the text captures the essential physics, a more detailed mechanism is being developed (M. Srinivasarao, J. O. Park, G. P. Neitzel, in preparation).
41. T. H. Dam, P. Pantano, *Rev. Sci. Instrum.* **70**, 3982 (1999).
42. J. S. Rossier, M. A. Roberts, R. Ferrigno, H. H. Girault, *Anal. Chem.* **71**, 4294 (1999).
43. J. Voldman, M. L. Gray, M. A. Schmidt, *Annu. Rev. Biomed. Eng.* **1**, 401 (1999).
44. S. John, *Phys. Rev. Lett.* **58**, 2486 (1987).
45. E. Yablonovitch, *Phys. Rev. Lett.* **58**, 2059 (1987).
46. J. D. Joannopoulos, R. D. Meade, J. N. Winn, *Photonic Crystals: Molding the Flow of Light* (Princeton Univ. Press, Princeton, NJ, 1995).
47. K. Busch, S. John, *Phys. Rev. Lett.* **83**, 967 (1999).

48. We thank P. Neitzel for many useful and educational discussions on thermocapillary convection, N. Allen for various discussions and use of her microscopy facilities, and especially C. Moreland for supporting this work both financially and morally. Supported by NSF grant DMR-0096240 through the CAREER program (M.S.).

29 November 2000; accepted 1 March 2001

Carbon Dioxide Degassing by Advective Flow from Usu Volcano, Japan

P. A. Hernández,[1,2]* K. Notsu,[1] J. M. Salazar,[2] T. Mori,[1] G. Natale,[1] H. Okada,[3] G. Virgili,[4] Y. Shimoike,[1] M. Sato,[1] N. M. Pérez[2]

Magmatic carbon dioxide (CO_2) degassing has been documented before the 31 March 2000 eruption of Usu volcano, Hokkaido, Japan. Six months before the eruption, an increase in CO_2 flux was detected on the summit caldera, from 120 (September 1998) to 340 metric tons per day (September 1999), followed by a sudden decrease to 39 metric tons per day in June 2000, 3 months after the eruption. The change in CO_2 flux and seismic observations suggests that before the eruption, advective processes controlled gas migration toward the surface. The decrease in flux after the eruption at the summit caldera could be due to a rapid release of CO_2 during the eruption from ascending dacitic dikes spreading away from the magma chamber beneath the caldera.

Usu volcano is one of the most active volcanoes in Japan, with seven major historic eruptions recorded since 1663. It is located on the northern coast of Funka-wan (Bay of Volcano) in the southwestern part of Hokkaido (Fig. 1) and consists of a basaltic edifice (49 to 53% SiO_2) with a small summit caldera and several dacitic lava domes and cryptodomes (68 to 73% SiO_2) on the summit and on its northern slope (*1*). The volcano is a postcaldera cone of Toya caldera, which is a nearly circular depression ~10 km in diameter, filled with Lake Toya. Boundaries of Lake Toya correspond to the Toya caldera rim. The summit of Usu consists of a small caldera, 1.8 km in diameter and ~500 m in elevation, covering a circular area ~7 to 8 km across the base. Domes and cryptodomes, aligned in two parallel zones running NW-SE, are probably controlled by the structure of the southern wall of Toya caldera, which is overlaid by Usu volcano. Historic volcanic eruptions are assumed to originate from episodic shallow dacitic intrusions, ascending from a deeper rhyolitic magma reservoir hypothesized to be at a depth of 10 km (*2*). The last eruption began on 7 August 1977, after 32 years of dormancy, and stopped in October 1978, forming the Usu-Shinzan cryptodome. Inter-eruptive activity consists of both fumarolic emissions distributed on the summit caldera and diffuse gas emanations spread over the volcanic edifice, together with persistent earthquake swarms.

Seismicity data observed by the Japan Meteorological Agency show an increasing number of volcanic earthquakes around Usu volcano since 1995. However, clear premonitory seismicity appeared at Usu on 28 March 2000, 3 days before the eruption (*3*). On 30 March, the ground began to rise in the area northwest of Nishi-yama and the north slope of Kompira-yama cryptodomes (Fig. 1), forming a new cryptodome due to a dike intrusion spreading northwest, away from a shallow dacitic magma chamber located at a depth of ~4 km beneath the summit caldera (*4*). The Usu Volcano Observatory Global Positioning System network detected upheaval over 2 m at the summit of Usu a few days before the eruption. The new cryptodome attained a maximum height of ~85 m (over the original altitude) on 10 July, and more than 50 craters formed in the area of ground uplift. The first crater was related to a phreatomagmatic eruption, followed by several phreatic eruptions.

CO_2 is the second-most abundant gas species released (after water), and the gas is generated mostly by subsurface magma-degassing bodies. As CO_2 travels upward by advective-diffusive transport mechanisms and manifests itself at the ground surface, changes over time in its flux pattern provide information about subsurface magma movement (*5–8*). For this reason, during this period (1998 to 2000) of unrest, three soil gas surveys were carried out, which focused mainly on the study of soil CO_2 (Table 1). The first survey was initiated in September 1998 under ideal weather conditions (no wind or clouds). These conditions provided minimal soil gas variations, thus eliminating disturbances such as soil moisture during the measurements. Atmospheric pressure slightly changed from 1019 to 1031 hPa during the survey. About 150 soil gas samples were

[1]Laboratory for Earthquake Chemistry, Graduate School of Science, University of Tokyo, Bunkyo-Ku 113-0033, Tokyo, Japan. [2]Environmental Research Division, Instituto Tecnológico y de Energías Renovables, 38611 Granadilla de Abona, Santa Cruz de Tenerife, Spain. [3]Usu Volcano Observatory, Hokkaido University, Sohbetsu-cho, Hokkaido 052-0103, Hokkaido, Japan. [4]WEST Systems, Via Molise 3, 56025 Pontedera (PI), Italy.

*To whom correspondence should be addressed. E-mail: phdez@iter.rcanaria.es